Powering Through Wildfires: An Integrated Solution for Enhanced Safety and Resilience in Power Grids

Mostafa Nazemi, *Graduate Student Member, IEEE*, and Payman Dehghanian, *Senior Member, IEEE*

***Abstract*—Safeguarding the nation's electrical infrastructure and personnel against natural and man-made disasters, and ensuring a continuous, reliable, and resilient supply of energy are among the top priorities for the electric industry. In recent years, wildfires have been remarkably threatening the safety and security of electric power grids demanding innovative frameworks for ensured resilience. Our proposed approach focuses on mitigation of wildfire disruptions that, once occur, can jeopardize the well-being of electrical equipment and the safety of the personnel. The proposed framework first offers a comprehensive wildfire characterization package that can spatiotemporally monitor and analyze the wildfire behaviors, i.e., wildfire intensity, arrival time, and binding paths from ignition points to electrical equipment. This allows power system operators to make proactive decisions before the fire approaches the electrical elements, e.g., power distribution lines. Next, a decision support tool for wildfire management in power grids is proposed such that various local generation resources,—i.e., distributed renewable energy resources and energy storage systems, can be effectively employed to mitigate the wildfire impacts on the power grid. The proposed integrated solution technology ensures a significant reduction in power outages and enhances the safety and resilience of the power grid and the operating personnel.**

***Index Terms*—Distributed energy resources, electrical safety, power distribution systems, resilience, wildfire hazards.**

NOMENCLATURE

A. Abbreviations

DLR	Dynamic line rating.
ESSs	Energy storage systems.
RESs	Renewable energy resources.
MTs	Micro-turbines.
PV	Photovoltaic energy.
WT	Wind turbine.
SoC	State of charge.

B. Sets and Indices

$i, j \in \mathbf{B}$	Indices/set of nodes (1 to N_B).
$ij \in \mathbf{L}$	Indices/set of power distribution branches connecting node i to j.
$ij \in \ell$	Indices/set of power distribution branches between node i and j affected by wildfire.
$t \in \mathbf{T}$	Indices/set of time periods (1 to N_T).

C. Parameters and Constants

1) Fire Parameters

T^f	Flame zone temperature (K).
l^f	Length of fire (m).
α^f	Tilt angle of fire (rad).
ρ^b	The bulk density of the fuel (kg/m^3).
ε^f	Flame zone emissivity.

2) Environmental Conditions

τ	Dimensionless atmospheric transmissivity.
B	Stefan-Boltzman constant (W/m^2˜K^4).
V^{wind}	Wind speed (m/s).
σ^{wind}	Angle between the wind direction and conductor axis (rad).
T^a	Ambient temperature (K).
k^a	Air thermal conductivity (W/mK).
μ^α	Dynamic viscosity of air (kg/ms).
ρ^α	Air density (kg/m^3).

3) Conductor Specifications

mC_p	Total heat capacity of conductor (J/mK).
D	Conductor diameter (mm).
∂	Solar absorptivity.
ϕ^{sun}	Solar radiation rate (W/m^2).
R^a_{ij}	Line ij resistance at the ambient temperature.
$T^{\max}$	Maximum permitted conductor temperature (K).

4) Price and Costs

VoLL	Value of lost load ($/MWh).
c^D	Selling electricity price ($/MWh).
c^{MT}	MTs generation cost ($/MW).
$c^{su/sd}$	MTs switching cost ($).

5) Power Distribution System Components

$P^{\text{d}}_{i,t}$	Active demanded power at node i at time t (MW).
$Q^{\text{d}}_{i,t}$	Reactive demanded power at node i at time t (MVar).
n^{ST}	Conversion efficiency of ESSs.
E^{ST}	Energy capacity of ESSs (MWh).

Manuscript received September 30, 2021; accepted March 5, 2022. Date of publication March 17, 2022; date of current version May 20, 2022. Paper 2021-ESafC-0679, presented at the 2021 Electrical Safety Workshop, Tucson, AZ, USA, Mar. 8–12, and approved for publication in the IEEE TRANSACTIONS ON INDUSTRY APPLICATIONS by the Electrical Safety Committee of the IEEE Industry Applications Society. This work was supported by the US National Science Foundation (NSF) under Grant ICER-2022505. *(Corresponding author: Mostafa Nazemi.)*

The authors are with the Department of Electrical and Computer Engineering, George Washington University, Washington, DC 20052 USA (e-mail: mostafa_nazemi@gwu.edu; payman@gwu.edu).

Color versions of one or more figures in this article are available at https://doi.org/10.1109/TIA.2022.3160421.

Digital Object Identifier 10.1109/TIA.2022.3160421

D. Functions and Variables

1) Fire Model

$\theta^f_{ij,t}$	Angle between approaching fire and line conductor ij at time t (rad).
$d^f_{ij,t}$	Distance between fire and line ij at time t (m).
V^f_t	Spread rate of fire at time t (m/s).
$T_{ij,t}$	Conductor temperature of line ij at time t (K).
ϕ^f_t	Radiative heat flux at time t (W/m^2).

2) Heat Gain and Loss

$q^{o}_{ij,t}$	Resistive heat gain rate of line ij at time t (W/m).
$q^{\text{sun}}_{ij,t}$	Solar heat gain rate of line ij at time t (W/m).
$q^{\text{fire}}_{ij,t}$	Fire heat gain rate of line ij at time t (W/m).
$q^{\text{con}}_{ij,t}$	Convective heat loss rate of line ij at time t (W/m).
$q^{\text{rad}}_{ij,t}$	Radiative heat loss rate of line ij at time t (W/m).

3) Power System Model

$p^D_{i,t}, q^D_{i,t}$	Active and reactive supplied power at node i at time t (MW, MVar).
$P^{\text{fl}}_{ij,t}, Q^{\text{fl}}_{ij,t}$	Active and reactive power flow on branch ij at time t (MW, MVar).
$\text{SoC}_{i,t}$	SoC of ESS at time t.
$p^{\text{Ch}}_{i,t}, p^{\text{DC}}_{i,t}$	Charging and discharging power of ESS at node i at time t (MW).
$q^{\text{ESS}}_{i,t}$	Reactive output power of ESS at node i at time t (MVar).
$p^{\text{MT}}_{i,t}, q^{\text{MT}}_{i,t}$	Active and reactive generated power of MT at node i (MW, MVar).
$P^{\text{WT}}_{i,t}, P^{S}_{i,t}$	Active generated power of WT and PV at node i at time t (MW).
$V_{\text{sqr}_{i,t}}$	Squared voltage at node i at time t (kV^2).
$p^{\text{shed}}_{i,t}, q^{\text{shed}}_{i,t}$	Active and reactive load shedding at node i at time t (MW, MVar).
p^{UP}_t	Active exchanged power with the upstream network at time t (MW).

E. Binary Variables

$\alpha_{ij,t}$	Line ij connection status at time t (1 if the line is connected, 0 otherwise).
$u_{i,t}$	ESS charging/discharging status at node i at time t (1 if charging, 0 otherwise).
$\gamma_{i,t}$	MT status at node i at time t (1 if the MT is online, 0 otherwise).
φ^{UP}_t	Buying/selling electricity from/to the up stream network at time t (1 if buying, 0 otherwise).

I. Introduction

A. Background and Motivation

WILDFIRE events have been continuously reported over the last decade in the United States. Despite spending \$2 to \$3 billion per year to assist wildland fire suppression operations, wildfires now cost the United States an estimated \$63 to \$285 billion in damages each year. In average, 62 805 wildfires have occurred every year from 2011 to 2020, impacting an average of 7.5 million acres. In 2020, 58 950 wildfires torched 10.1 million acres, the second-highest acreage burned in a single year since 1960; approximately 40% of these acres were in California [1]. Driven by climate change consequences, the impacts of weather on wildfires include, but are not limited to, behavior (wind speed and direction), fuels (combustible material), and ignitions (lightning). Wildfires are also significantly influenced by relative humidity, which is controlled by temperature, precipitation, and other climatic parameters, all of which are potentially influenced by climate change. Continued climate change will further worsen the situation, as higher temperature and changed precipitation would cause fuels to be more flammable for extended periods of time, potentially affecting the magnitude, frequency, and severity of wildfires. These evolving circumstances may jeopardize the well-being of electrical infrastructure (e.g., power plants, transmission, and distribution lines) and the personnel safety [2].

Electric power networks and wildfire hazards are remarkably intertwined demanding further safety considerations. In general, the likelihood of a fire being started directly by electric equipment is minimal (usually around 1.5% of all ignitions) [3]; however, during droughts and hot seasons, the percentage of fires caused by electrical equipment increases substantially, reaching up to 30% of the overall ignitions [3]. Power system failures can occur for a variety of causes, the most common of which are tree/vegetation/bush-related problems. It has been reported that fallen trees or branches, typically from trees beyond the electric utility's right-of-way, cause 80% of all vegetation-related problems in power networks [4]. This may result in breakage of the power line conductors. Electric current may run over an extended period of time with high energy, causing the vegetation to dry, resulting in high-temperature arcing and, finally, igniting a fire. Therefore, as a precaution, electricity might be shut off in high-risk wildfire regions during extreme weather events (e.g., high intensity wind) for public safety in an effort to avert a fast-moving, difficult-to-control wildfire. On the other hand, power line-related impacts from wildfires are not limited to the actual destruction of the structures. In the event of a large wildfire, there are several minor or moderate fires with a long front length causing thermal stress to overhead power lines and jeopardizing their integrity. In such circumstances, the capacity of the conductor can be indirectly influenced by the heat and smoke, even if there is no severe damage to the tower physically [5]. Accordingly, the power line will be most likely out of service, which results in load outages with severe financial losses. There is, hence, an urgent need to enrich the electrical safety and resilience of power delivery infrastructure while reducing and mitigating wildfire threatening risks.

B. Literature Review

Several efforts in the literature have focused on the wildfires as a threat to power systems. Reference [6] provides a comprehensive overview of the challenges, consequences, and potential methods for reducing wildfire risk in power systems. Various technical solutions to minimize or prevent the wildfires caused by power system elements are comprehensively reviewed

in [7]. An optimization approach is introduced in [8] to make a balance between power shut-offs and wildfire risk. Particularly, the suggested model optimizes the power grid operation to maximize electricity delivery to end customers while proactively reducing the risk of wildfire by selectively de-energizing some portions of the system. A general framework is suggested in [9] to characterize the probability of wildfire ignitions caused by faults in the electric network. Dynamic line rating (DLR) of overhead lines is proposed in [10] to model the impact of wildfire on the temperature of the overhead lines. It shows that the overhead power line might be out of service due to excess heat gained from the approaching fire when the temperature of the conductor exceeds the maximum allowable temperature. A unified model is proposed in [11] that integrates the fire heat transfer model with the dynamic rating of overhead lines. The suggested model includes the radiative and convective heat generated by a progressing wildfire in order to obtain the updated conductor rating. The thermal stress of overhead conductors is modeled in [12], where the temperature rise of conductors is obtained based on wildfire parameters. Dian *et al.* [13] proposed an integrated wildfire early warning framework for power networks that combines wildfire prediction with early warning of line outage likelihood. An optimal strategy for dispatching the extinguishing equipment in electric grids is introduced in [14], where the interaction between fire and electric grid is modeled with a dynamic game in which wildfire aims to maximize the loss of the electric grid, whereas the goal of the electric grid is to limit the losses. In summary, although several research have studied the wildfire modeling and its consequences on power systems, the literature lacks further exploration of spatial-temporal fire behavior, mitigation mechanisms, and integrated safety solutions in case of wildfire extremes.

C. Relevance to Electric Safety

Electric safety is primarily defined as the preventative and proactive actions required to ensure the safety of network infrastructures and the operating personnel in face of emergency incidents. Particularly, the integrity of power distribution lines becomes a challenge in the face of wildfires (even small fires), since the radiative and convective heat put additional heat stress on the conductors, which result in temperature rise of power line conductors. Once the overhead power distribution line faces an approaching wildfire, the conductor can be cooled down by taking the line out of service. This helps take out the resistive heat resulted from the flowing electricity, also mitigating the safety concerns for the operating personnel. In this regard, the overhead distribution lines have to be taken out of service in an optimal time, i.e., neither very soon nor very late, to prevent conductors from melting on one hand and having the minimum power outages on other hand. To overcome the load outages due to unavailability of some power distribution branches, all local resources, i.e., Renewable energy resources (RESs), Energy storage systems (ESSs), Microturbines (MTs), should be then operated in an optimal and cost-efficient manner. To magnify the importance of electric network resilience and safety, therefore, this article aims to integrate the spatiotemporal wildfire behavior and characteristics into an optimization framework to manage the network optimally in the face of a progressive wildfire. This article provides the power system operators with a framework for optimal operation of all local resources in face of wildfire incidents to minimize the load outages and boost power system resilience.

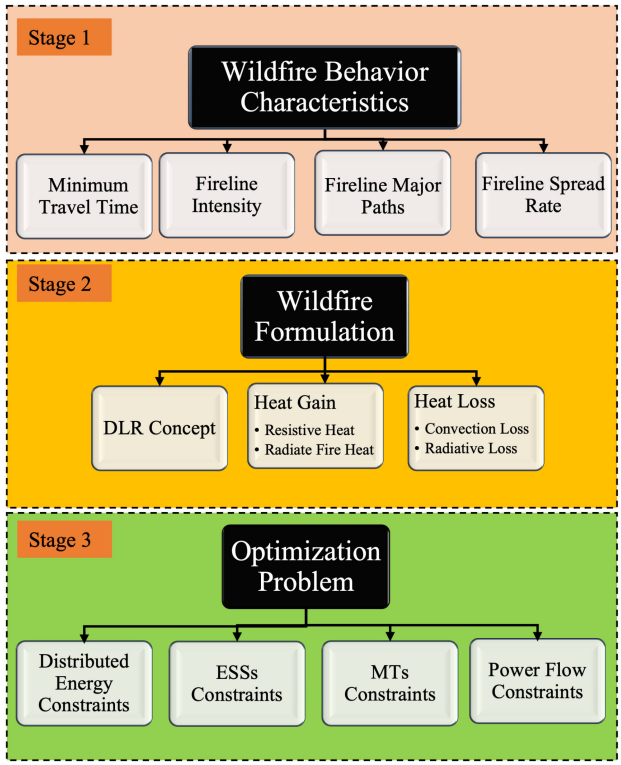

Fig. 1. Big-picture of the proposed framework.

The rest of this article is organized as follows. Section II introduces the big picture of the proposed framework. The fire behavior is modeled in Section III and is formulated in Section IV. The problem formulation for optimal system operation during wildfire events is presented in Section V. Numerical case study and simulation results on a modified IEEE 33-bus test system are demonstrated in Section VI. Finally, Section VII concludes this article.

II. Big Picture of the Proposed Framework

The big picture of the proposed framework is illustrated in Fig. 1. The proposed framework consists of three interconnected stages. A comprehensive mechanism for spatiotemporal wildfire analyses is developed using the IFTDSS platform [15] in Stage 1—see Fig. 1. The IFTDSS platform uses a new quantitative risk index that can capture the role of vegetation, fuel, weather parameters including wind speed and wind direction, number of ignitions, and the location of each ignition on wildfire propagation. The next step is to assess the vulnerability of power system elements in the face of wildfire hazards; hence, the power grid is mapped to the geographical landscape and wildfire analyses layers—see Fig. 2. In Stage 2, we propose

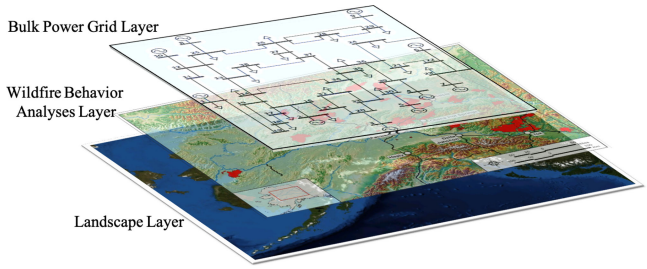

Fig. 2. Mapping bulk power grid layer to landscape and fire analyses layers.

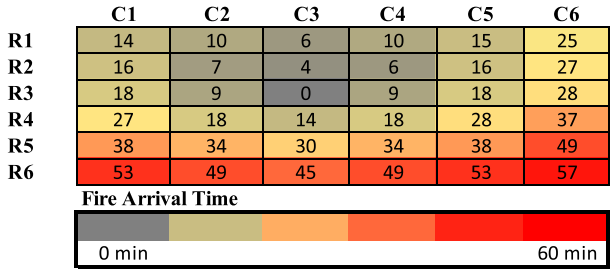

Fig. 3. Fire arrival times (min) for a 6 × 6 cell landscape.

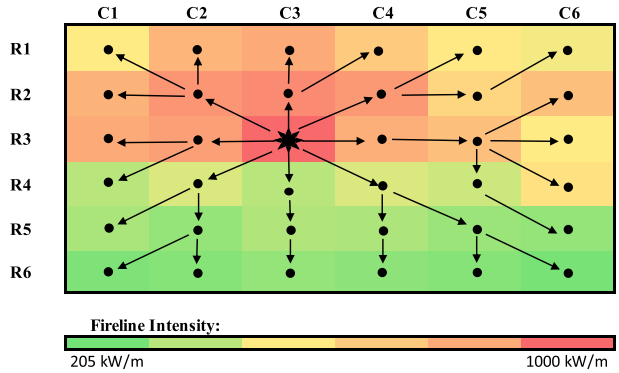

Fig. 4. Fire spread paths and fire line intensity for a 6 × 6 cell landscape.

to emulate wildfire events based on their common impact on power systems: the sharp decrease in the availability of system elements. For large fires, we propose to use simplified heat flux emitted from the fire to a conductor. The applied formulation ensures that every related parameter and the calculated heat from the fire are sufficiently accurate. The next step is to add the dynamic rating model and formulations of the overhead power lines. The overhead temperature of distribution line can increase remarkably in case of wildfires. If the temperature surpasses the threshold, the line will be considered out of service, which can cause some load outages. The heat transferred from fire to the conductor has to be added to other sources that raise the conductor temperature. Hence, the proposed formulation accommodates the changes in conductor temperature by using the nonsteady-state heat balance equations. Finally, in Stage 3, the proposed optimization problem is formulated where different constraints related to power system operation and fire behavior are modeled, integrated, linearized, and then convexified to be solved by off-the-shelf optimization solvers. Mining of these spatial-temporal relationships enables targeted emergency safety response actions and the optimal allocation of limited resources ensuring resilience.

III. Fire Behavior Modeling

Inspired by [16], this section is dedicated to fire behavior modeling that can analyze the spatial-temporal fire behavior. The presented model here is able to compute both fire line intensity and minimum fire arrival time based on the direction that a fire spreads from the ignition point. The first step to model fire behavior is to realize wildfire characteristics and parameters. Wind speed, wind direction, fuel model, elevation, slope, canopy cover, and fuel moisture among others are the parameters that can determine the severity of wildfires. Nodes are here referred to points at the center of each cell on a landscape. According to spatial connection equations, each node must be lit precisely once by fire from surrounding nodes along a fire spread route or can be also ignited by exogenous ignitions [16]

$$D_i + \xi_i \geq \zeta_i + \frac{1}{n_i} \sum_{j \in \omega_i} D_j \quad \forall i \tag{1}$$

where D_i is binary indicator: $D_i = 1$ if node i is burnt and $D_i = 0$ otherwise; ξ_i is binary parameter indicating whether node i is flammable (0) or not; $\zeta_i = 1$ indicates if the fire is ignited from node i; n_i is the number of nodes adjacent to node i, and ω_i is the set of nodes adjacent to node i. $\sum_{j \in \omega_i} B_{ji} = D_i - \zeta_i$ should be also considered, which indicates that if node i burns, only one fire spread path into it is identified; the model only considers the first time that fire reaches to the node. B_{ji} is a binary indicator: $B_{ji} = 1$ indicates that binding fire spread path into node i was from node j. The set of fire spread equations track the required time that it takes fire spreading between two different individual nodes. To compute the fire arrival time, fire arrival time equations have to be used. Fire line intensity is also determined based on some equations using the binding spread path that fire arrives at each node ($I_i = \sum_j k_{ji} B_{ji} + k_i \zeta_i \ \ \forall i$), where I_i has to be considered a decision variable reflecting the fire line intensity; k_{ji} is fire line intensity from node j to node i; and k_i indicates the fire line intensity if the fire ignited in node i [16].

The fire behavior is modeled and analyzed here using the IFTDSS platform [15]. An example is provided to illustrate 6 × 6 completely flat and homogenous cell landscape [16]. This simplified landscape can mimic the fire behavior, where it has some gentle to moderate slopes and the north is considered at the top of both figures. Given the wind blowing from the south to the north, Fig. 3 illustrates the fire arrival time for each node considering the ignition point (C3, R3). Fig. 4 shows the binding fire spread paths and fire line intensities. The fire line intensity changes depending on the wind degree. For example, the fire line intensity at (C3, R2) is high because fire spread path from (C3, R3) to node (C3, R2) is perfectly parallel to the anticipated wind direction, whereas the intensity of fire is much lower at node (C3, R4) since the fire spread path is directly against the wind. The same ideology is used later in this article using the IFTDSS

platform to characterize the fire spatial-temporal behavior at the location of power distribution branches.

IV. Wildfire Modeling Formulation

A. Wildfire Model

The wildfire model applied here has been originally proposed in [10]. Heat from wildfires is generally transmitted by radiation and convection. Convective transmission is not of our concern in this article, since it impacts the temperature of the conductors only when the fire is exactly under the overhead conductors. In such situations, when fire is in a close distance with the overhead lines, the lines will be out of service. On the other hand, when the fire is far from the line, the radiative heat transferred from fire to a conductor has to be modeled accurately, since it impacts the temperature of the conductor which might jeopardize the acceptable safety of the line. The radiative heat flow ϕ^f from the approaching flame is then computed using the shape of the flame and the fire front characteristics as follows:

$$\phi^f_{ij,t} = \frac{\tau \cdot \varepsilon^f \cdot B \cdot T^{f^4}}{2} \cdot \sin(\theta^f_{ij,t}) \tag{2}$$

where τ, ε^f, and B are all environmental parameters. T^f is the temperature of the fire front and θ^f is the view angle between the impacted line and the approaching fire front indicated as

$$\theta^f_{ij,t} = \tan^{-1}\left(\frac{l^f \cdot \cos(\alpha^f)}{d^f_{ij,t} - (l^f \cdot \sin(\alpha^f))}\right) \tag{3}$$

where l^f represents the fire length and d^f is the distance between fire and the affected conductor computed in (4)

$$d^f_{ij,t} = d^f_{ij,t-1} \cdot V^f_t \cdot \Delta t \cdot \cos(\sigma^{\text{wind}}_{ij,t}) \tag{4}$$

$$V^f_t = \frac{b \cdot (1 + V^{\text{wind}}_t)}{\rho^b}. \tag{5}$$

V^f(m/s) is the spread rate of wildfire on a flat surface depending on the wind speed V^{wind}(m/s). ρ^b is the bulk density of the fuel and b is a constant [11].

B. On the Concept of DLR

The calculation of the power line conductor temperature is presented based on [10]. The fire heat gain q^{fire} is added to other source of heats, i.e., solar heat gain rate q^{sun}, and the resistive heat of the line q^o. Convective heat loss rate q^{con} and the radiative heat loss rate q^{rad} are the sources of heat loss, which cool down the conductor temperature. Fig. 5 illustrates different types of heat gain and loss for a power line conductor. Thus, all variations in temperature at every time period are computed using the nonsteady-state heat equation

$$(T_{ij,t+1} - T_{ij,t}) = \frac{\Delta t}{mC_p} \cdot (q^o_{ij,t} + q^{\text{sun}}_{ij,t} + q^{\text{fire}}_{ij,t} - q^{\text{con}}_{ij,t} - q^{\text{rad}}_{ij,t}). \tag{6}$$

Each of the above terms are explained as follows.

1) Heat Gain: In the given equation, the solar heat that the conductor may absorb, the resistive thermal heat made by the current running through the power line conductor, and the radiative heat by fire are all measured as follows:

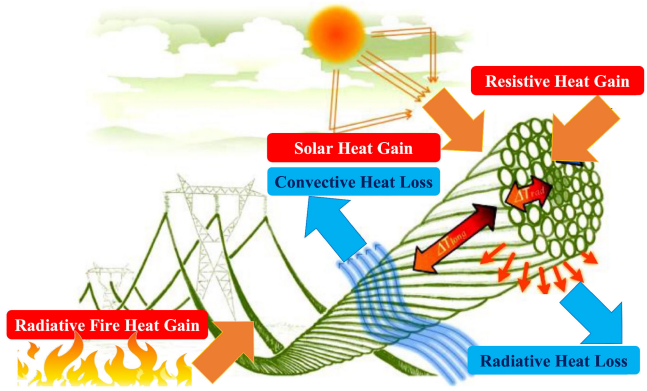

Fig. 5. Illustration of different types of heat gain and heat loss for power line conductors in the event of a wildfire [17].

$$q^{\text{sun}}_{ij,t} = D_{ij} \cdot \partial_{ij} \cdot \phi^{\text{sun}}_{ij,t} \tag{7}$$

$$q^o_{ij,t} = R^{\text{line}}(T_{ij,t}) \cdot (I_{ij,t})^2 \tag{8}$$

$$q^{\text{fire}}_{ij,t} = D_{ij} \cdot \phi^{\text{fire}}_{ij,t}. \tag{9}$$

In (7), D_{ij} indicates the conductor diameter and $\phi^{\text{sun}}_{ij,t}$ is the sun radiation rate while the solar absorptivity reflected by ∂_{ij} varies between 0.27 and 0.95 depending on the type of conductors. A value of 0.5 is otherwise used if no information is available for conductor absorptivity [18]. In (8), the function between the conductor resistance and the associated conductor temperature is established by $R^{\text{line}}(T_{ij,t})$

$$R^{\text{line}}(T_{ij,t}) = R^a_{ij} \cdot (1 + d_{ij} \cdot (T_{ij,t} - T^a)). \tag{10}$$

R^a_{ij} represents the conductor resistance in ambient temperature T^a (298°K) and d_{ij} indicates the coefficient associated to the thermal resistance of conductor.

2) Heat Loss: The last two terms in (6) represent the cooling down factors of the conductor. In this article, the convection loss is considered as the power line is cooled by a cylinder of flowing air around the conductor. The convection heat loss varies depending on wind speed according to the IEEE standard [19]. Equations (11) represents the calculation of the convection loss

$$q^{\text{con}}_{ij,t} = \max\begin{pmatrix} K^\theta_{ij,t} \cdot [1.01 + 1.35 \cdot N^{0.52}_{ij,t}] \cdot k^a \cdot (T_{ij,t} - T^a) \\ K^\theta_{ij,t} \cdot 0.754 \cdot N^{0.6}_{ij,t} \cdot k^a \cdot (T_{ij,t} - T^a) \end{pmatrix} \tag{11}$$

where N is the Reynolds number and K^θ is wind direction factor calculated as follows:

$$N_{ij,t} = \frac{D_{ij} \cdot \rho^\alpha \cdot V^{\text{wind}}_t}{\mu^\alpha} \tag{12}$$

$$K^\theta_{ij,t} = 1.194 - \cos(\sigma^{\text{wind}}_{ij,t}) + 0.194\cos(2\sigma^{\text{wind}}_{ij,t}) + 0.368\sin(2\sigma^{\text{wind}}_{ij,t}). \tag{13}$$

The radiated heat loss rate is presented as follows:

$$q_{ij,t}^{\text{rad}} = 17.8 D_{ij} \cdot \epsilon \cdot \left[\left(\frac{T_{ij,t}}{100} \right)^4 - \left(\frac{T^a}{100} \right)^4 \right]. \quad (14)$$

Detailed information is additionally available in [10].

V. Problem Formulation

A. Wildfire Mitigation Optimization Problem

Based on [10] and [20], a linear optimization model is used to ensure the safety and resilient supply of energy to critical loads in the face of progressive wildfires. Operating costs are considered to ensure the most cost-effective operation solution during a progressive wildfire. Therefore, the objective function is designed to minimize the total cost as indicated below

$$\begin{aligned} \min \Bigg(& \sum_{t=1}^{N_T} \sum_{i=1}^{N_B} (\text{VoLL} \cdot p_{i,t}^{\text{shed}} - c^D \cdot p_{i,t}^D) \\ & + \sum_{t=1}^{N_T} \sum_{i=1}^{N_B} (c^{\text{MT}} \cdot p_{i,t}^{\text{MT}}) + \sum_{t=1}^{N_T} \sum_{i=1}^{N_B} (su_{i,t}^{\text{MT}} + sd_{i,t}^{\text{MT}}) \Bigg) \\ & + \sum_{t=1}^{N_T} c_t^{\text{UP}} \cdot (p_t^{\text{UP}_B} - p_t^{\text{UP}_S}). \end{aligned} \quad (15)$$

In the first line, $\text{VoLL} \cdot p_{i,t}^{\text{shed}}$ represents the load shedding cost and $c^D \cdot p_{i,t}^D$ indicates the revenue from supplying energy to the customers. The second and third terms reflect the generation and start-up/shut-down costs associated to MTs. The last term expresses the cost related to buying/selling energy from/to the upstream network. To optimally operate the electric distribution grid in the face of progressive wildfire events, multiple constraints should be considered as described in the following.

1) Distributed Energy Constraints: RESs, i.e., wind and solar energy, can be employed to supply portions of the network when the fire hits the distribution grid. To tackle the uncertain nature of RESs, the Weibull and von Mises distributions are considered. It is supposed that wind speed V^{wind} has the following probability distribution:

$$f(V^{\text{wind}}) = \frac{K^0}{C^k} \cdot V^{K^0-1} \cdot e^{(-V/C)^{K^0}} \quad (16)$$

where K^0 and C are the parameters associated to the Weibull distribution. The relationship between the generated energy by WTs and the wind speed can be modeled as follows:

$$P_{i,t}^{\text{WT}} = 0, \ 0 \le V \le V_{\text{ci}} \quad \text{or} \quad V_{\text{co}} \le V \quad \forall i \in \mathbf{B}, t \in \mathbf{T} \quad (17)$$

$$P_{i,t}^{\text{WT}} = P_{\text{r}}^w \cdot \left(\frac{V - V_{\text{ci}}}{V_r - V_{\text{ci}}} \right), V_{\text{ci}} \le V \le V_r \quad \forall i \in \mathbf{B}, t \in \mathbf{T} \quad (18)$$

$$P_{i,t}^{\text{WT}} = P_{\text{r}}^w, \quad V_r \le V \le V_{\text{co}} \quad \forall i \in \mathbf{B}, t \in \mathbf{T}. \quad (19)$$

where V is the wind speed at the height of the WTs; V_{ci}, V_{co}, and V_r are, respectively, the cut-in wind speed, the cut-out wind speed, and the rated wind speed; and P_{r}^w is the rated output of wind generation units [21].

Regarding solar energy, the illumination intensity is commonly regarded as the most important element influencing the output power of the solar panel. The following describes the relationship between the intensity of light and the output power of a PV unit:

$$P_{i,t}^S = P_{\text{r}}^S \cdot \left(\frac{S}{S_r} \right), \quad 0 \le S \le S_r, \forall i \in \mathbf{B}, t \in \mathbf{T} \quad (20)$$

$$P_{i,t}^S = P_{\text{r}}^S, S_r \le S, \forall i \in \mathbf{B}, t \in \mathbf{T} \quad (21)$$

where S is the illumination intensity, S_r is the rated value, and P_{r}^S indicates the rated output power of PV units.

2) MTs Constraints: To ensure the power distribution system runs at the minimum possible cost, the active and reactive output power of MTs as well as their start-up/shut-down costs must be considered as follows:

$$p_{i(\text{min})}^{\text{MT}} \cdot \gamma_{i,t} \le p_{i,t}^{\text{MT}} \le p_{i(\text{max})}^{\text{MT}} \cdot \gamma_{i,t} \quad \forall i \in \mathbf{B}, t \in \mathbf{T} \quad (22)$$

$$q_{i(\text{min})}^{\text{MT}} \cdot \gamma_{i,t} \le q_{i,t}^{\text{MT}} \le q_{i(\text{max})}^{\text{MT}} \cdot \gamma_{i,t} \quad \forall i \in \mathbf{B}, t \in \mathbf{T} \quad (23)$$

$$sd_{i,t}^{\text{MT}} \ge c_i^{sd} \cdot (\gamma_{i,t-1} - \gamma_{i,t}) \ge 0 \quad \forall i \in \mathbf{B}, t \in \mathbf{T} \quad (24)$$

$$su_{i,t}^{\text{MT}} \ge c_i^{su} \cdot (\gamma_{i,t} - \gamma_{i,t-1}) \ge 0 \quad \forall i \in \mathbf{B}, t \in \mathbf{T} \quad (25)$$

where (22) and (23) determine the maximum and minimum limits for active and reactive power of MTs, respectively; constraints (24) and (25) indicate the start up and shut down costs of the MTs, respectively. The binary variable $\gamma_{i,t}$ is applied to determine the online/offline status of MTs, i.e., 1 for start up and 0 for shut down, where the corresponding costs c_i^{sd} and c_i^{su} are considered the same.

3) ESSs Constraints: The operation constraints of ESSs can be expressed as follows:

$$\text{SoC}_{i,t} = \text{SoC}_{i,t-1} + \left(\frac{n_i^{\text{ST}} \cdot p_{i,t}^{\text{Ch}} \cdot (\frac{\Delta t}{3600})}{E_i^{ST}} \right) - \left(\frac{p_{i,t}^{\text{DC}} \cdot (\frac{\Delta t}{3600})}{n_i^{\text{ST}} \cdot E_i^{\text{ST}}} \right) \quad \forall i \in \mathbf{B}, t \in \mathbf{T} \quad (26)$$

$$\text{SoC}_{i,(\text{min})} \le \text{SoC}_{i,t} \le \text{SoC}_{i,(\text{max})} \quad \forall i \in \mathbf{B}, t \in \mathbf{T} \quad (27)$$

$$0 \le p_{i,t}^{\text{Ch}} \le p_{i,t,(\text{max})}^{\text{Ch}} \cdot u_{i,t} \quad \forall i \in \mathbf{B}, t \in \mathbf{T} \quad (28)$$

$$0 \le p_{i,t}^{\text{DC}} \le n_i^{\text{ST}} \cdot p_{i,t,(\text{max})}^{\text{DC}} \cdot (1 - u_{i,t}) \quad \forall i \in \mathbf{B}, t \in \mathbf{T} \quad (29)$$

$$q_{i(\text{min})}^{\text{ESS}} \le q_{i,t}^{\text{ESS}} \le q_{i(\text{max})}^{\text{ESS}} \quad \forall i \in \mathbf{B}, t \in \mathbf{T} \quad (30)$$

$$\text{SoC}_{i,t_{\text{end}}} \ge \text{SoC}^\star \quad \forall i \in \mathbf{B}. \quad (31)$$

In the equations above, constraint (26) calculates the SoC of ESSs. Constraint (27) limits the SoC of ESSs at each time interval. The charged and discharged powers of ESSs are always between zero and their maximum value determined in constraints (28) and (29). The reactive power is limited by constraint (30). Constraint (31) is to guarantee that the SoC of ESSs is always higher than a predefined level $\text{SoC}^\star$ at the end of time horizon t_{end}.

4) Power Flow Constraints: At each node, there should be a balance between the generated and demanded electricity as

shown in constraints (32) and (33).

$$\sum_{j=1}^{N_{B_i}} P_{ij,t}^{\text{fl}} = p_{i,t}^{\text{MT}} + p_{i,t}^{\text{WT}} + p_{i,t}^{S} + p_{t}^{\text{UP}} + p_{i,t}^{\text{Ch}} - p_{i,t}^{\text{DC}} - p_{i,t}^{D}$$
$$\forall i \in \mathbf{B}, t \in \mathbf{T} \tag{32}$$

$$\sum_{j=1}^{N_{B_i}} Q_{ij,t}^{\text{fl}} = q_{i,t}^{\text{MT}} + q_{i,t}^{\text{Ch}} - q_{i,t}^{D} \quad \forall i \in \mathbf{B}, t \in \mathbf{T} \tag{33}$$

$$-\underline{P}_{ij,t}^{\text{fl}} * \alpha_{ij,t} \le P_{ij,t}^{\text{fl}} \le \bar{P}_{ij,t}^{\text{fl}} * \alpha_{ij,t} \quad \forall i \in \mathbf{B}, t \in \mathbf{T} \tag{34}$$

$$-\underline{Q}_{ij,t}^{\text{fl}} * \alpha_{ij,t} \le Q_{ij,t}^{\text{fl}} \le \bar{Q}_{ij,t}^{\text{fl}} * \alpha_{ij,t} \quad \forall i \in \mathbf{B}, t \in \mathbf{T}$$

$$V_{\text{sqr}_{i,t}} - V_{\text{sqr}_{j,t}} \le (1-\alpha_{ij,t}) \cdot M_1 + 2 \cdot (r_{ij} \cdot P_{ij,t}^{\text{fl}} + x_{ij} \cdot Q_{ij,t}^{\text{fl}}), \quad \forall ij \in \mathbf{L}, t \in \mathbf{T} \tag{35}$$

$$V_{\text{sqr}_{i,t}} - V_{\text{sqr}_{j,t}} \ge (\alpha_{ij,t} - 1) \cdot M_1 + 2 \cdot (r_{ij} \cdot P_{ij,t}^{\text{fl}} + x_{ij} \cdot Q_{ij,t}^{\text{fl}}), \quad \forall ij \in \mathbf{L}, t \in \mathbf{T} \tag{36}$$

$$\underline{V_{\text{sqr}_i}} \le V_{\text{sqr}_{i,t}} \le \overline{V_{\text{sqr}_i}}, \quad \forall i \in \mathbf{B}, t \in \mathbf{T}. \tag{37}$$

Constraints (34) and (35) let the electricity run through each line only when the line is online, i.e., $\alpha_{ij,t} = 1$. Constraints (36) and (37) illustrate the power flow relations according to the DistFlow equations [22]. M_1 is a large-enough positive number to relax these two constraints for offline branches. Voltage magnitude of each node is bounded in constraint (38).

The variables $p_{i,t}^{D}$ and $q_{i,t}^{D}$ are the supplied active and reactive power to the customers, which are computed by the load shedding $p_{i,t}^{\text{shed}}$ subtracted from the original demand at each node $P_{i,t}^{\text{d}}$ in (39) and (40).

$$p_{i,t}^{D} = P_{t}^{\text{d}} - p_{t}^{\text{shed}} \quad \forall i \in \mathbf{B}, t \in \mathbf{T} \tag{39}$$

$$q_{t}^{D} = Q_{t}^{\text{d}} - q_{t}^{\text{shed}} \quad \forall t \in \mathbf{T} \tag{40}$$

$$0 \le p_{i,t}^{\text{shed}} \le P_{i,t}^{\text{d}} \quad \forall i \in \mathbf{B}, t \in \mathbf{T} \tag{41}$$

$$q_{i,t}^{\text{shed}} = p_{i,t}^{\text{shed}} \cdot \frac{Q_{i,t}^{\text{d}}}{P_{i,t}^{\text{d}}} \quad \forall i \in \mathbf{B}, t \in \mathbf{T} \tag{42}$$

In constraint (32), the active power p_t^{UP} represents the energy purchases from or sold to the upstream network and needs to be bounded as shown in constraints (43)–(45).

$$p_{t}^{\text{UP}} = p_{t}^{\text{UP}_{\text{buy}}} - p_{t}^{\text{UP}_{\text{sell}}} \quad \forall t \in \mathbf{T} \tag{43}$$

$$0 \le p_{t}^{\text{UP}_{\text{buy}}} \le p_{\text{max}}^{\text{UP}_{\text{buy}}} \cdot \varphi_{t}^{\text{UP}} \quad \forall t \in \mathbf{T} \tag{44}$$

$$0 \le p_{t}^{\text{UP}_{\text{sell}}} \le p_{\text{max}}^{\text{UP}_{\text{sell}}} \cdot (1 - \varphi_{t}^{\text{UP}}) \quad \forall t \in \mathbf{T}. \tag{45}$$

5) DLR Constraints: The following constraints determine the change in the temperature of overhead power lines.

$$(T_{ij,t+1} - T_{ij,t}) = \frac{\Delta t}{mC_p} \cdot \left[(q_{ij,t}^{\varrho} + q_{ij,t}^{\text{sun}} + q_{ij,t}^{\text{fire}} - q_{ij,t}^{\text{con}} - q_{ij,t}^{\text{rad}}) \right] \quad \forall ij \in \ell, t \in \mathbf{T} \tag{46}$$

$$q_{ij,t}^{\text{sun}} = D_{ij} \cdot \partial_{ij} \cdot \phi_{ij,t}^{\text{sun}} \quad \forall ij \in \ell, t \in \mathbf{T} \tag{47}$$

$$q_{ij,t}^{\varrho} = R^{\text{line}}(T_{ij,t}) \cdot (I_{ij,t})^2 \quad \forall ij \in \ell, t \in \mathbf{T} \tag{48}$$

$$q_{ij,t}^{\text{fire}} = D_{ij} \cdot \phi_{ij,t}^{\text{fire}} \quad \forall ij \in \ell, t \in \mathbf{T} \tag{49}$$

$$q_{ij,t}^{\text{con}} = \max \begin{pmatrix} K_{\text{angle}} \cdot [1.01 + 1.35 \cdot N_{Re}^{0.52}] \cdot k^a \cdot (T_{ij,t} - T^a) \\ K_{\text{angle}} \cdot 0.754 \cdot N_{Re}^{0.6} \cdot k^a \cdot (T_{ij,t} - T^a) \end{pmatrix} \tag{50}$$

$$q_{ij,t}^{\text{rad}} = 17.8 D_{ij} \cdot \epsilon \cdot \left[\left(\frac{T_{ij,t}}{100} \right)^4 - \left(\frac{T^a}{100} \right)^4 \right] \quad \forall ij \in \ell, t \in \mathbf{T} \tag{51}$$

$$T_{ij,t} \le T^{\text{max}} + (1 - \alpha_{ij,t}) * M_2 \quad \forall ij \in \ell, t \in \mathbf{T} \tag{52}$$

$$\alpha_{ij,t} \le \alpha_{ij,t-1} \quad \forall ij \in \ell, t \in \mathbf{T} \tag{53}$$

Constraint (46) indicates the nonsteady-state heat balance. Constraints (47)–(49) show the heat gain by the conductor, whereas constrains (50) and (51) demonstrate the heat loss by the conductor. Constraint (52) reflects that when the temperature of the conductor surpasses the maximum permitted conductor temperature, the associated overhead line will be out of service. To achieve electrical safety, once the overhead line gets unavailable, it will remain out of service for the rest of the time horizon as shown in constraint (53).

B. Convexification and Linearization

The resistive losses, presented in (48), are the multiplication of current flow square and conductor resistance. For an ohmic conductor, as shown in (10), the resistance can be represented as a function of conductor temperature. To convexify the resistive heat, it is assumed that the the conductor resistance is constant and equals to its maximum at the maximum permissible temperature T^{max}. In addition, the voltage is approximately assumed to be 1 p.u. Accordingly, constraint (48) is relaxed to the following inequality.

$$q_{ij,t}^{\varrho} \ge R^{\text{line}}(T^{\text{max}} \cdot (|P_{ij,t}^{\text{fl}}|^2 + |Q_{ij,t}^{\text{fl}}|^2)). \tag{54}$$

The radiation heat loss can be rewritten as a function of the difference between the conductor temperature and the ambient temperature times a slope [10].

$$q_{ij,t}^{\text{rad}} = a \cdot T_{ij,t} + b \tag{55}$$

where a and b are the associated coefficients (see [20] for more information).

VI. Case Study and Numerical Results

A. Test System Properties and Simulation Data

A modified IEEE 33-node test system [23] is considered to show the effectiveness of the applied framework for resilient operation of the power distribution grids in the face of wildfires.

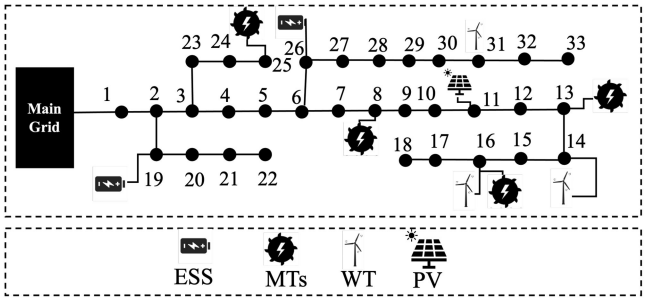

Fig. 6. Modified IEEE 33-node test system (extracted from [10]).

The single-line diagram of the considered test system is illustrated in Fig. 6. The test system is assumed to be a balanced distribution grid with active peak demand equal to 13.35 MW. The location of ESSs, MTs, and RESs are depicted in Fig. 6 and the data on the distribution system components are taken from [10]. The cut-in, cut-out, and rated wind speeds for WTs are 4, 20, and 12 m/s, respectively. The PV panels have a rated illumination intensity of 1000 W/m2. Weather parameters are derived from [11] and the wind and solar data are taken from [24] and [25]. Wind speed and solar radiation have the standard deviation equal to 15% of the mean value while loads have the standard deviation equal to 5% of the mean value. The von Mises distribution is supposed to have a k-factor of 2 [10]. This article only focuses on the first 24 h of the emergency period and is composed of time steps of 1 h duration. The temperature of the fire front is set as 1200°K [26] and the initial distance of the fire from the affected power lines is assumed as 1200 m. It is also assumed that the affected lines will be out of service until the end of the time horizon. The SoC of the ESSs is expected to be more than 30% of the full potential, in order to contribute to demand fulfillment for the next hours after the analysis. The type of conductors is considered as aluminum conductor steel reinforced (ACSR) and the diameter and the maximum acceptable temperature of the power line is considered equal to 21 mm and 353 °K, respectively. All other data can be found in [10] and [20]. We have used IFTDSS platform [15] to generate the spatiotemporal fire behavior. The model type in the software is considered as minimum travel time (MTT) fire spread. The landscape is considered to be 945 acres and is located in northern California. The wind type is Gridded Winds and the wind speed is considered as 15 mph. Wind direction is assumed to be 0. Scott/Reinhardt is considered for crown fire method and the foliar moisture is assumed to be 100. The spotting probability is considered 20%. The initial fuel moisture parameters are considered as follows: 5 for 1 h, 10 for 10 h, 15 for 100 h, 40 for live herbaceous fuel moisture, and 70 for live wood fuel moisture. The optimization problem is performed using CPLEX solver to handle the optimization formulation. The numerical analysis of the results is performed on a PC with an Intel Xeon E5-2620 v2 processor, 16 GB of memory, and a 64-b operating system using a general algebraic modeling system.

B. Fire Safety and Resilient Operation

The proposed framework is applied to optimize the power distribution network operation with the aim of enhancing wildfire safety and resilience. The spatial-temporal characteristics of the fire are simulated in Fig. 7. The power distribution system nodes mapped onto the landscape are also presented in Fig. 7(f). One can notice that based on the input data, the fire burns in five different burn periods which will result in load outages in different time intervals. Fire arrival time and fire line intensity for each single node of the test system are shown, respectively, in Figs. 8 and 9. Note that each cell is associated to each node. For instance, node 1 is associated to cell (R1, C1); node 14 is associated to cell (R3, C2); node 28 is associated to cell (R5, C4), etc. One can realize that the fire arrival time to the power nodes varies between 14 and 60 h. The fire line intensity varies between 60 to 1300 kW/m. Based on the obtained fire line intensity and arrival time, power lines: 1-2, 2-3, 3-4, 3-23, and 2-19 are going to be impacted for the first 24 h. The fire arrival time, the optimal unavailability time, and the conductor temperature before unavailability of the impacted lines are tabulated in Table I. It is observed that before fire actually arrives to a close distance, e.g., 300 m, of the line, the temperature of the line exceeds the maximum threshold and, as a result, the line will be out of service for the rest of the time horizon. One can realize that the obtained unavailability time of the impacted distribution lines by approaching the wildfire helps prevent the resistive heat, and as a result, the temperature of conductors does not increase exponentially, which enhances the safety and integrity of power distribution lines. Fig. 10 illustrates the energy exchange with the upstream network, the total generated energy from WT and solar panels, as well as the total generated energy from MTs for the first 24 h. It is observed that before 11:00, the energy is bought from the upstream network since the renewable cannot fully meet the demand and also the cost of local MTs is much higher than that of buying electricity form the upstream network. After 11:00, the role of MTs and ESSs become more important due to the unavailability of line 1-2 at 11:00, which makes the network isolated from the upstream network. For instance, the ESS at node 26 gets charged from 1:00 to 8:00 as shown in Fig. 11 and remain in its fully charged capacity until 15:00. After 15:00 until 24:00, the ESS gets discharged to supply the critical loads depending on the VoLL value of each load. From 11:00 to 24:00, the average generated energy from MTs, WT, and solar are, respectively, 7.079 MWh, 2.039 MWh, and 179.18 kWh while the average demand in those time intervals is 12.29 MWh. The spatial load shedding is depicted in Fig. 12. It is observed that the minimum load shedding is 1.8208 MW at 24:00, while the maximum load shedding is 3.4383 MW at 12:00. One can also realize that before the isolation of the network at 12:00, no load shedding was recorded. It is observed that even with the existence of MTs and RESs, a big portion of loads has to

TABLE I
IMPACTED LINES BY AN APPROACHING WILDFIRE (FIRST 24 H)

Lines	Fire Arrival Time	Optimal Unavailability Time	Line Temperature before Unavailability
1-2	14.00	11:00	351 °K
2-3	16.00	11:00	340 °K
3-4	16.00	14:00	344 °K
3-23	15:00	11:00	350 °K
2-19	17:00	15:00	330 °K

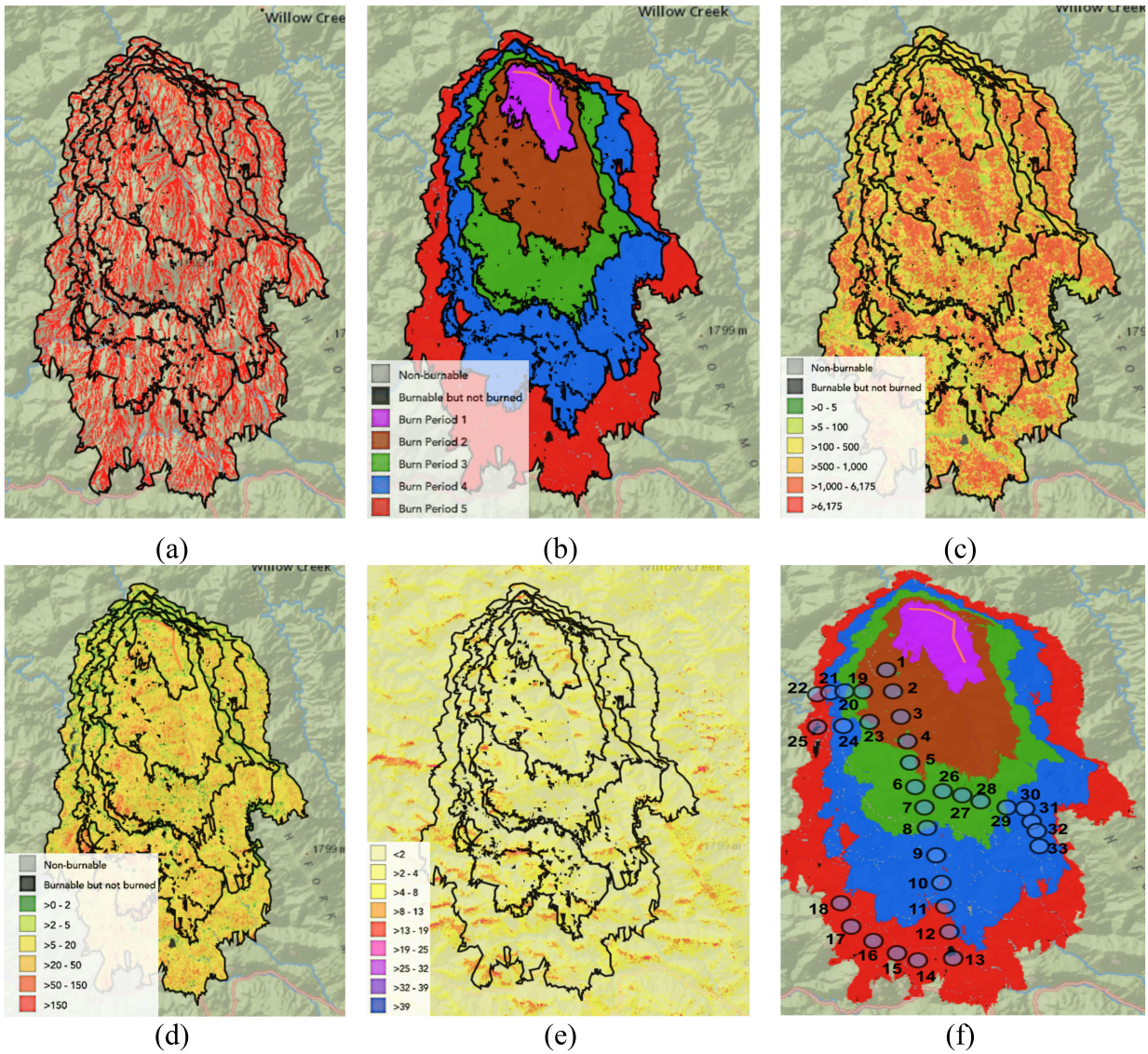

Fig. 7. Spatial-temporal wildfire characteristics obtained for the case study. (a) Minimum Travel Time (MTT) major paths indicated with red color; (b) MTT arrival time; (c) MTT fire line intensity (BTU/10ft-sec); (d) MTT rate of spread (chains/hr); (e) Midflame wind speed (mph); and (f) the case study mapped onto the studied landscape.

	C1	C2	C3	C4	C5	C6
R1	14.1	16.9	19.5	23.2	28.1	29.1
R2	27.2	37	42.5	47.8	53	49.3
R3	58.2	54.8	55.2	51.7	54.2	50.2
R4	26.6	38.3	45.7	58.6	24	44.3
R5	58.9	31.3	28.6	29.8	35.4	38.4
R6	39.5	40.5	41.9			

Fire Arrival Time

0 min 60 hr

Fig. 8. Fire arrival times for the studied case.

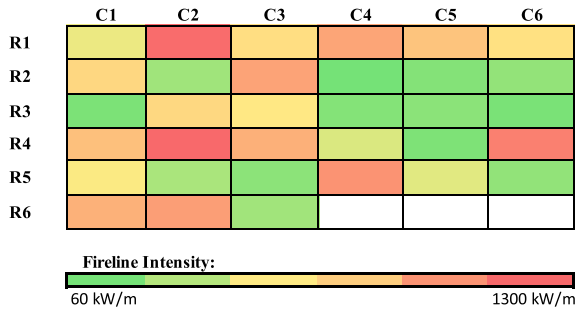

Fig. 9. Fire line intensity for the studied case.

be shed at the isolated part of the network; however, it can be ensured that the load shedding costs maintain at its minimum level by optimizing the use of local resources. Table II presents the objective function, the load shedding cost, the generation costs by MTs, the power exchange cost, and the revenue from selling energy to the end customers. The VoLL is here considered

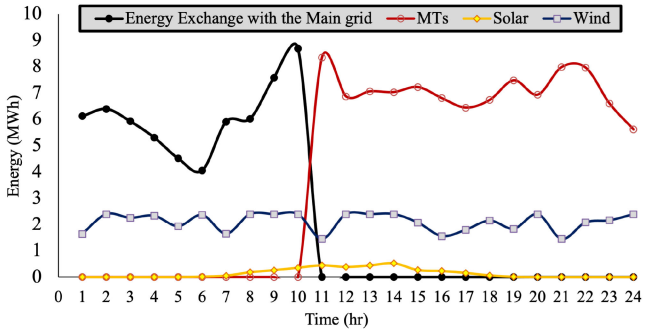

Fig. 10. Total energy exchange with the upstream network, total available renewable energy, and total energy generated by MTs in the first 24 h.

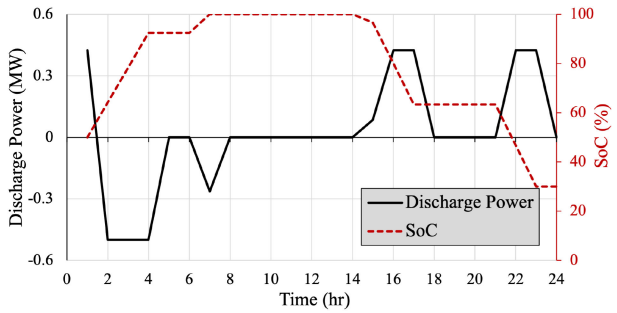

Fig. 11. Discharging power and SoC of ESS at node 26 in the first 24 h.

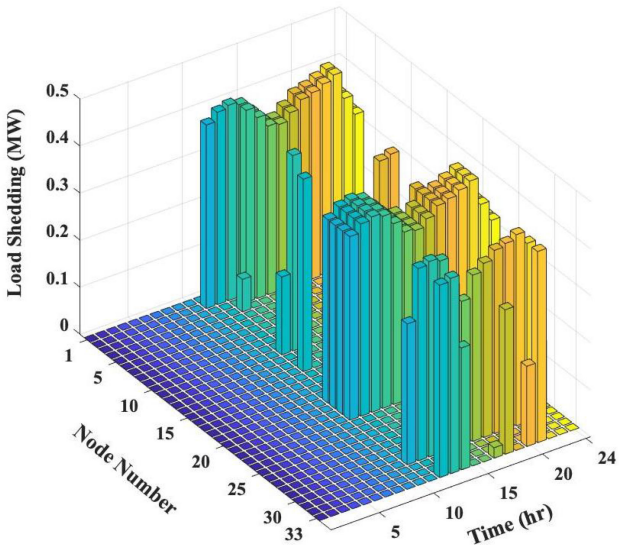

Fig. 12. Spatial load shedding in the first 24 h.

TABLE II
REVENUE AND ASSOCIATED COSTS FOR THE FIRST 24 H ($\$\times 10^3$)

Objective Function	Load Shedding Cost	Generation Cost	Power Exchange Cost	Revenue from Selling Energy to Customers
-8.8166	38.3189	9.1284	1.5833	57.8471

as 1000 $/MWh [10], [27] to supply prioritized loads first. It can be observed that the higher the load shedding, the lower the revenue from selling energy to end customers resulting in a higher objective function. In summary, one can observe that in the face of massive fires, the electrical safety is highly dependent on how much time in advance power system operators are provided with the unavailability time of distribution lines and how optimally the local resources can be employed.

VII. CONCLUSION

This article presented an effective framework that leverages all available local resources, i.e., RESs, MTs, and ESSs, in case of massive wildfires to enhance the the electrical safety and operational resilience. The applied operation solution functionality integrates various aspects of wildfire into the optimization to quantitatively model the impact of wildfire on the overhead distribution lines. The concept of DLR is applied to imitate the dynamic temperature of conductors and find the optimal unavailability time of impacted lines to ensure their safety by taking out of resistive heats and preventing them from melting. An mixed-integer linear programming (MILP) optimization formulation is applied to find the optimal operation of local resources and to ensure the distribution operational resilience in case of approaching wildfires. The numerical results revealed that the load outages due to unavailability of impacted lines in different time periods could be remarkably reduced if the progressive wildfire is spatially temporally characterized in advance and all local resources are strategically and optimally coordinated. Future research can be focused on first enriching the proposed approach by developing fire fragility functions of power distribution equipment, second, developing a multistochastic fire-safety approach to tackle the stochasticity of weather parameters that could change the wildfire behavior characteristics, and third, investigating the prescribed wildfire tools to enhance the safety of power systems and operating staffs by reducing the fuels and preventing a destructive fire.

REFERENCES

[1] "The congressional research service, wildfire statistics," 2021. [Online] Available: https://sgp.fas.org/crs/misc/IF10244.pdf
[2] J. A. Sathaye *et al.*, "Rising temps, tides, and wildfires: Assessing the risk to california's energy infrastructure from projected climate change," *IEEE Power Energy Mag.*, vol. 11, no. 3, pp. 32–45, May/Jun. 2013.
[3] B. G. Teague, R. N. McLeod, and S. M. Pascoe, "Final report, 2009 victorian bushfires royal commission," Parliament of Victoria, Australia, 2010.
[4] B. D. Russell, C. L. Benner, and J. A. Wischkaemper, "Distribution feeder caused wildfires: Mechanisms and prevention," in *Proc. 65th Annu. Conf. Protective Relay Engineers*, 2012 pp. 43–51.
[5] S. Jazebi, F. de León, and A. Nelson, "Review of wildfire management techniques-Part I: Causes, prevention, detection, suppression, and data analytics," *IEEE Trans. Power Del.*, vol. 35, no. 1, pp. 430–439, Feb. 2020.
[6] J. W. Muhs, M. Parvania, and M. Shahidehpour, "Wildfire risk mitigation: A paradigm shift in power systems planning and operation," *IEEE Open Access J. Power Energy*, vol. 7, pp. 366–375, 2020.
[7] S. Jazebi, F. de León, and A. Nelson, "Review of wildfire management techniques-Part II: Urgent call for investment in research and development of preventative solutions," *IEEE Trans. Power Del.*, vol. 35, no. 1, pp. 440–450, Feb. 2020.

[8] N. Rhodes, L. Ntaimo, and L. Roald, "Balancing wildfire risk and power outages through optimized power shut-offs," *IEEE Trans. Power Syst.*, vol. 36, no. 4, pp. 3118–3128, Jul. 2021.
[9] J. Muhs, M. Parvania, H. T. Nguyen, and J. A. Palmer, "Characterizing probability of wildfire ignition caused by power distribution lines," *IEEE Trans. Power Del.*, vol. 36, no. 6, pp. 3681–3688, Dec. 2020.
[10] D. N. Trakas and N. D. Hatziargyriou, "Optimal distribution system operation for enhancing resilience against wildfires," *IEEE Trans. Power Syst.*, vol. 33, no. 2, pp. 2260–2271, Mar. 2018.
[11] M. Choobineh, B. Ansari, and S. Mohagheghi, "Vulnerability assessment of the power grid against progressing wildfires," *Fire Saf. J.*, vol. 73, pp. 20–28, 2015.
[12] E. I. Koufakis, P. T. Tsarabaris, J. S. Katsanis, C. G. Karagiannopoulos, and P. D. Bourkas, "A wildfire model for the estimation of the temperature rise of an overhead line conductor," *IEEE Trans. Power Del.*, vol. 25, no. 2, pp. 1077–1082, Apr. 2010.
[13] S. Dian *et al.*, "Integrating wildfires propagation prediction into early warning of electrical transmission line outages," *IEEE Access*, vol. 7, pp. 27586–27603, 2019.
[14] Z. Jian, J. Guo, and X. Xu, "Optimal dispatch strategy analysis of fire extinguishing equipment for electric grid wildfire based on dynamic game," *Int. Trans. Elect. Energy Syst.*, vol. 30, no. 4, 2020, Art. no. e12264.
[15] US Department of the Interior & US Department of Agriculture, 2021, "Interagency fuels treatment decision support system (IFTDSS)," 2021. [Online] Available: https://iftdss.firenet.gov/
[16] E. J. Belval, Y. Wei, and M. Bevers, "A mixed integer program to model spatial wildfire behavior and suppression placement decisions," *Can. J. Forest Res.*, vol. 45, no. 4, pp. 384–393, 2015.
[17] A. Ahmadi, M. Nabipour, B. Mohammadi-Ivatloo, and V. Vahidinasab, "Ensemble learning-based dynamic line rating forecasting under cyberattacks," *IEEE Trans. Power Del.*, vol. 37, no. 1, pp. 230–238, Feb. 2022.
[18] I. Z. F. bin Hussien, A. A. Rahim, and N. Abdullah, "Electric power transmission," in *Alternative Energy in Power Electronics*, Amsterdam, The Netherlands: Elsevier, pp. 317–347, 2011.
[19] *IEEE Standard for Calculating the Current-Temperature Relationship of Bare Overhead Conductors*, IEEE Std 738-2012 (Revision of IEEE Std 738-2006 - Incorporates IEEE Std 738-2012), pp. 1–72, 2013.
[20] M. Nazemi, P. Dehghanian, M. Alhazmi, and Y. Darestani, "Resilient operation of electric power distribution grids under progressive wildfires," *IEEE Trans. Ind. Appl.*, vol. 58, no. 2, pp. 1632–1643, Mar./Apr. 2022.
[21] Z. Liu, F. Wen, and G. Ledwich, "Optimal siting and sizing of distributed generators in distribution systems considering uncertainties," *IEEE Trans. Power Del.*, vol. 26, no. 4, pp. 2541–2551, Oct. 2011.
[22] M. E. Baran and F. F. Wu, "Network reconfiguration in distribution systems for loss reduction and load balancing," *IEEE Trans. Power Del.*, vol. 4, no. 2, pp. 1401–1407, Apr. 1989.
[23] C. Wang and H. Z. Cheng, "Optimization of network configuration in large distribution systems using plant growth simulation algorithm," *IEEE Trans. Power Syst.*, vol. 23, no. 1, pp. 119–126, Feb. 2008.
[24] D. Papaioannou, C. Papadimitriou, A. Dimeas, E. Zountouridou, G. Kiokes, and N. Hatziargyriou, "Optimization & sensitivity analysis of microgrids using homer software-a case study," in *Proc. MedPower*, 2014, pp. 1–7.
[25] National Renewable Energy Laboratory (NERL), [Online]. Available: http://pvwatts.nrel.gov
[26] J.-L. Rossi, A. Simeoni, B. Moretti, and V. Leroy-Cancellieri, "An analytical model based on radiative heating for the determination of safety distances for wildland fires," *Fire Saf. J.*, vol. 46, no. 8, pp. 520–527, 2011.
[27] S. Mohagheghi and S. Rebennack, "Optimal resilient power grid operation during the course of a progressing wildfire," *Int. J. Elect. Power Energy Syst.*, vol. 73, pp. 843–852, 2015.
[28] M. Nazemi and P. Dehghanian, "Powering through wildfires: An integrated solution for enhanced safety and resilience in power grids," in *Proc. IEEE IAS Elect. Saf. Workshop*, 2021.

Mostafa Nazemi (Graduate Student Member) received the B.Sc. degree in electrical engineering from the K. N. Toosi University of Technology, Tehran, Iran, in 2015, and the M.Sc. degree in energy systems engineering from the Sharif University of Technology, Tehran, Iran, in 2017. He is currently working toward the Ph.D. degree in electrical engineering with the Department of Electrical and Computer Engineering, George Washington University, Washington, DC, USA.

His research interests include power system resilience, power system planning and operation, energy optimizations, and smart electricity grid applications.

Nazemi was the recipient of the 2018 Certificate of Excellence in Reviewing by the Editorial Board Committee of the Journal of Modern Power and Clean Energy for his contributions to the journal.

Payman Dehghanian (Senior Member, IEEE) received the B.Sc. degree in electrical engineering from University of Tehran, Tehran, Iran, in 2009, the M.Sc. degree in electrical engineering from Sharif University of Technology, Tehran, Iran, in 2011, and the Ph.D. degree, in electrical engineering from Texas A&M University, Texas, USA, in 2017.

He is an Assistant Professor with the Department of Electrical and Computer Engineering, George Washington University, Washington, D.C., USA. His research interests include power system protection and control, power system reliability and resiliency, asset management, and smart electricity grid applications.

Dr. Dehghanian is the recipient of the 2014 and 2015 IEEE Region 5 Outstanding Professional Achievement Awards, and the 2015 IEEE-HKN Outstanding Young Professional Award, and the 2021 Early Career Award from the Washington Academy of Sciences.